Automatic Alignment of Standard Views in 3D Echocardiograms Using Real-time Tracking

Fredrik Orderud[a], Hans Torp[a] and Stein Inge Rabben[b]

[a]Norwegian University of Science and Technology (NTNU), Trondheim, Norway;
[b]GE Vingmed Ultrasound, Oslo, Norway

ABSTRACT

In this paper, we present an automatic approach for alignment of standard apical and short-axis slices, and correcting them for out-of-plane motion in 3D echocardiography. This is enabled by using real-time Kalman tracking to perform automatic left ventricle segmentation using a coupled deformable model, consisting of a left ventricle model, as well as structures for the right ventricle and left ventricle outflow tract. Landmark points from the segmented model are then used to generate standard apical and short-axis slices. The slices are automatically updated after tracking in each frame to correct for out-of-plane motion caused by longitudinal shortening of the left ventricle.

Results from a dataset of 35 recordings demonstrate the potential for automating apical slice initialization and dynamic short-axis slices. Apical 4-chamber, 2-chamber and long-axis slices are generated based on an assumption of fixed angle between the slices, and short-axis slices are generated so that they follow the same myocardial tissue over the entire cardiac cycle. The error compared to manual annotation was 8.4 ± 3.5 mm for apex, 3.6 ± 1.8 mm for mitral valve and $8.4 \pm 7.4°$ for apical 4-chamber view. The high computational efficiency and automatic behavior of the method enables it to operate in real-time, potentially during image acquisition.

1. INTRODUCTION

Numerous tools for quantitative analysis of 3D echocardiograms have appeared over the last years, especially for left ventricular assessment. But despite all this innovation, visual wall-motion analysis still remains one of the most important clinical procedures in assessment of cardiac function. Traditionally, assessment of cardiac segments were time consuming, since several apical and parasternal 2D recordings had to be acquired independently, and examined successively to assess regional cardiac function.

With 3D echocardiography, arbitrary image slices can be extracted from acquired volumes. 3D echocardiography scanners incorporate tools to align and extract non-foreshortened apical 4-chamber (A4C), 2-chamber (A2C) and long-axis slices (LAX), as well as several short-axis slices. All cardiac segments can then be visualized simultaneously, based on a single 3D recording with sector wide enough to cover the entire ventricle.[1]

Existing tools require manual alignment of the left ventricular long-axis, which increases the examination time. More seriously, the resulting slices remain at fixed spatial positions within the image volume throughout the cardiac cycle. This means that the myocardial tissue being displayed differs during the cardiac cycle. This is especially a problem for basal short-axis slices, where the longitudinal shortening may be up to 1.2 cm during the cardiac cycle. The resulting out-of-plane motion can give rise to artificial wall thickening unrelated to cardiac contraction, and basal slices can end up in the atria at systole.

Several approaches for automatic identification of the left ventricular orientation have previously been published. Veronesi have published an optical-flow approach for measurement of the long-axis,[2] and Stralen have published a similar paper,[3] based on a combination of Hough-transform with dynamic programming. In addition, some approaches that also identify apical view orientation in addition to the long-axis have also been published. Lu has presented a database-driven approach for the detection of standard view planes,[4] and Leung have presented an approach for registration of stress echocardiography that also identify left ventricular orientation.[5] All of these studies did, however, report computational costs in the order of minutes per cardiac cycle, which makes them unsuitable for real-time operation. The results published by Veronesi[2] were also limited to analyzing the length of the long-axis, whereas Stralen also compared the long-axis angle.[3] None of the latter papers reported any position error for apex or base. Instead, they reported aggregate results based on comparison in every frame in each recording in the dataset, which makes comparison difficult.

In this paper, we present a method for automatically generating anatomically corrected short-axis slices, as well as automatically aligned standard apical views. The short-axis slices are evenly spaced between the apex and base of a fitted deformable model, whereas the apical view are aligned based on the orientation of the model, with a fixed angle between the slices. The slices are also automatically corrected for out-of-plane motion to ensure that the same myocardial tissue is imaged throughout the cardiac cycle. Due to the high computational efficiency, the method is able to operate in real-time, potentially during image acquisition.

2. METHODS

Automatic alignment of standard views are achieved by fitting several coupled deformable models to cardiac structures using a computationally efficient tracking framework previously described.[6,7] This framework used an extended Kalman filter[8] to perform temporal predictions, and assimilate edge-detection measurements from each model to compute a Bayesian least squares fitting of the models in a non-iterative fashion. Landmarks are then extracted from the fitted models, and subsequently used as basis for the extraction of aligned standard views.

2.1 Coupled deformable models

Automatic alignment of cardiac views requires information about both the ventricular long-axis, as well as the circumferential orientation of the heart. Usage of a left ventricle (LV) model alone is not believed to suffice, since circumferential information extracted from such a model would have to be based solely on the asymmetrical properties of the shape, which can vary greatly between subjects and depending on pathology. An alternative approach is to use coupled models to simultaneously track several cardiac structures. This allows for more reliable assessment of orientation, by computing the angle between the LV model and the different structures.

To ensure clear and unambiguous detection of both the long-axis and circumferential orientation, we therefore combine a LV model with a sail-like structure for the inferior right ventricular wall (RV), as well as a tube-like structure for the left ventricular outflow tract (OT). A deformable Doo-Sabin subdivision surface[9] is used as LV model, as described in.[6] For the RV, the inferior RV wall is selected since this is the part of the right ventricle that is usually most visible, whereas the anterior wall often suffers from drop-out. All models share a global transform (G) for translation, rotation and scaling. The OT model is also addition connected to a hinge transform (H), which allows the model to rotate to adapt to inter-subject differences in anatomy for the outlet tract.

Fig. 1(a) illustrates how the models are arranged in relationship to one another in a tracking hierarchy, whereas Fig. 2(b) illustrates the relative geometric configuration between the models after fitting in a typical recording.

A state-space representation of the tracking hierarchy can be constructed by concatenating the parameters from all transforms and models into a state vector, as described in.[7] The RV sail and OT cylinder does not have any shape parameters and are only affected by their associated transforms, so the concatenated state vector therefore becomes $\mathbf{x} = \begin{bmatrix} \mathbf{x}_g^T & \mathbf{x}_{lv}^T & \mathbf{x}_h^T \end{bmatrix}^T$.

2.2 Tracking framework

The overall tracking framework for coupled models is based on the framework introduced in,[6,7] with most steps very similar and therefore only briefly presented in this paper. The primary difference is that steps 2 through 4 are performed independently for each model in the tracking hierarchy as shown in Fig. 1(b), instead of only for a single model. The 5 steps can be summarized as:

1. Temporal prediction of the composite state vector $\bar{\mathbf{x}}_{k+1} = f\left(\hat{\mathbf{x}}_k,\ \mathbf{x}_0\right)$ based on the updated state from previous frame and a prediction function f, with associated increase in the covariance matrix. The temporal function is typically a linear auto-regressive model.

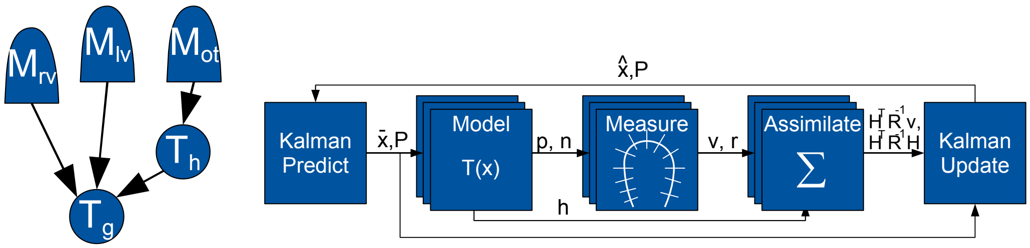

(a) (b)

Figure 1: (a) Tracking hierarchy for the deformable models, showing the global transform T_g, LV model M_{lv}, RV-sail M_{rv}, hinge transform T_h, as well as the LV outlet tract T_{ot}. (b) Flowchart over the Kalman tracking framework.

2. Evaluation of surface points $\mathbf{p}$, normal vectors $\mathbf{n}$ and Jacobian matrices $\mathbf{J}$ for all models in the tracking hierarchy, based on the predicted state $\bar{\mathbf{x}}_k$ as described in.[6]

3. Detection of normal displacement measurements v, measurement noise r and measurement vectors $\mathbf{h} = \mathbf{n}^T\mathbf{J}$, based on edge detection in the image volume, relative to surface points from the predicted models.

4. Assimilate measurement results from each model by summing the results in information space: $\mathbf{H}^T\mathbf{R}^{-1}\mathbf{v} = \sum_i \mathbf{h}_i r_i^{-1} v_i$, $\mathbf{H}^T\mathbf{R}^{-1}\mathbf{H} = \sum_i \mathbf{h}_i r_i^{-1} \mathbf{h}_i^T$.

5. Compute an updated state estimate, based on the prediction and measurement information: $\hat{\mathbf{x}}_k = \bar{\mathbf{x}}_k + \hat{\mathbf{P}}_k\mathbf{H}^T\mathbf{R}^{-1}\mathbf{v}_k$, $\hat{\mathbf{P}}_k^{-1} = \bar{\mathbf{P}}_k^{-1} + \mathbf{H}^T\mathbf{R}^{-1}\mathbf{H}$.

Tracking can be performed fully automatic, and initialized by placing a model with average shape in the center of the image sector. Edge-detection measurement are performed in each frame to detect the endocardial wall in search normals distributed evenly across the surface. Parameters for the shape of the model is combined with parameters for global translation, rotation and scaling to form a state-space representation of the segmentation problem.

2.3 Model-based alignment

Landmark points from the fitted models are used to generate standard apical and short-axis slices. The slices are automatically updated after tracking in each frame to correct for out-of-plane motion caused by longitudinal shortening of the left ventricle.

During tracking, landmark points from apex and base of the LV model are extracted from the segmented model after fitting in each frame. The angles between the LV model, the RV sail and OT cylinder is also computed to infer circumferential orientation of the heart. This orientation is then used to automatically generate standard apical 4-chamber, 2-chamber and long-axis views centered through the apex-base long-axis vector as seen in figure 2(a). The views are aligned circumferentially oriented based on an assumption of a 60 degree angle between the slices. In addition, evenly distributed short-axis slices orthogonal to the apex-base long-axis are generated, as seen in figure 2(b). The position of these slices is updated after tracking in each frame to correct the slices for out-of-plane motion caused by longitudinal shortening of the left ventricle.

3. RESULTS

The real-time tracking framework was used to perform left ventricular segmentation in a collection of 35 3D echocardiography recordings, preselected so that over 70% of the myocardium was visible (38% exclusion rate). Furthermore, they were all acquired with the convention that the azimuth view shown on the screen during volume acquisition should approximately resemble a A4C view to limit the inter-recording variability in probe orientation.

Tracking was implemented to process the acquired spherical grayscale data directly, and consumed approximately 7 ms processing time per frame (2.16GHz Intel core 2 duo processor). This makes the framework capable

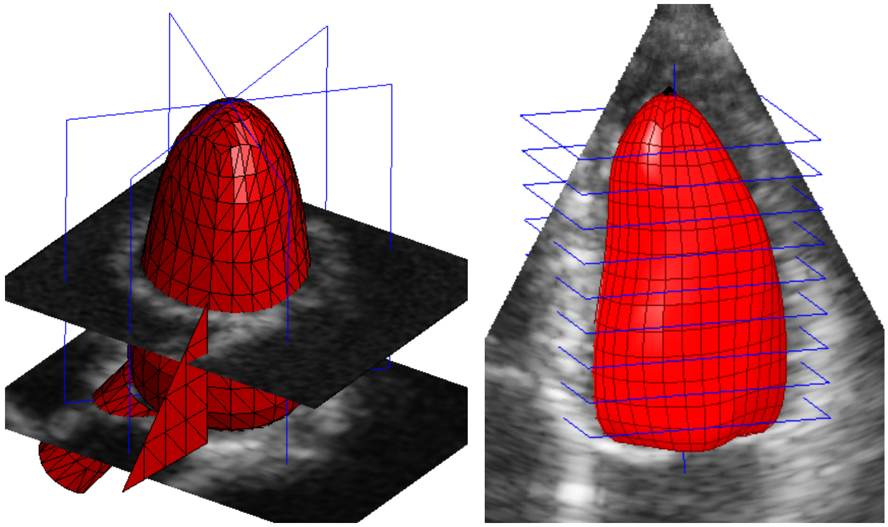

(a) Apical alignment (b) Short-axis alignment

Figure 2: Example illustrations of automatic model-based alignment: (a) Extraction of standard apical views based landmarks from the coupled LV-models. (b) Extraction of short-axis slices, based on the long-axis of the LV model.

	Apex	Base/Mitral valve
Position error	8.4 ± 3.5 mm	3.6 ± 1.8 mm

Table 1: Position errors for the apex and base compared to manual landmarks. Values are expressed as mean absolute distance $\pm$ SD in millimeters.

of operating in real-time. Automatically generated views and landmarks from the fitted models in all 35 recordings were compared to landmarks from manual image annotation at end-diastole conducted by an independent operator.

3.1 Alignment examples

Landmarks from apex and base was then retrieved from the fitted models in all frames to align the short-axis slices. Figure 3 compares the results of using fixed short-axis slices with dynamic slices that compensate for out-of-plane motion between end-diastole (ED) and end-systole (ES) in an example recording. Notice the distinctive difference in the basal slices, which when not corrected images the atria during systole. For mid-wall slices, the same part of the papillary muscles appear to be tracked in the dynamic slices. This is contrasted by the fixed mid-wall slices, where the papillary muscles move in and out of the slice.

Figure 4 shows an example of automatically extracted standard 4-chamber, 2-chamber and long-axis apical views, based on landmarks from the fitted models. The figure also shows detected long-axis and circumferential orientation (yellow), compared to the long-axis and orientation from manual image annotation (white).

3.2 Alignment errors

Figure 1 and 2 shows the results of quantitative comparison of the automatically extracted views and landmark points to the manually annotated reference. Position errors are given in absolute Cartesian distances, and angle errors are given as absolute rotation angle diffences for a plane through the long-axis. Bias values are also reported for the average signed angle errors, and say something about consistent deviation in one direction.

4. DISCUSSION

A novel approach for automating and improving the generation of standard apical and anatomic short-axis slices from 3D echocardiograms has been presented. Usage of the approach is believed to both automate positioning

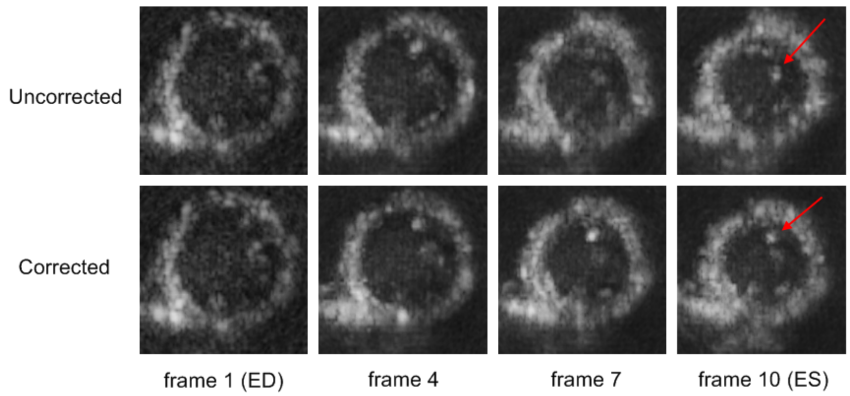

(a) Mid-wall slices

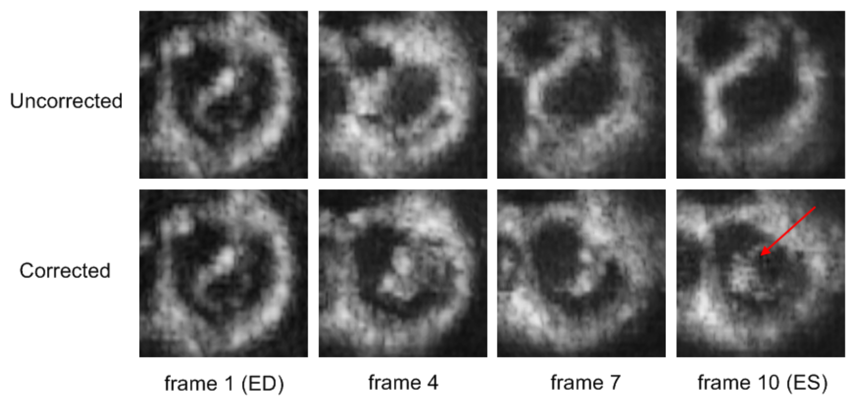

(b) Basal slices

Figure 3: Example uncorrected and corrected short-axis slices from the mid-wall (a) and base (b) of the left ventricle. Notice how the papillary muscles (arrows) appear more similar in the corrected mid-wall slices, and how the mitral valve (red arrow) is followed in the corrected basal slices.

	A4C	A2C	LAX
Rotation error	$8.4 \pm 7.4°$	$8.0 \pm 7.6°$	$11.8 \pm 8.5°$
Bias	$0.3°$	$1.1°$	$-7.9°$

Table 2: Rotation errors for the standard apical views compared to views inferred from manual landmarks. Values are expressed as mean absolute error ± SD in degrees. Bias is the average signed angle error.

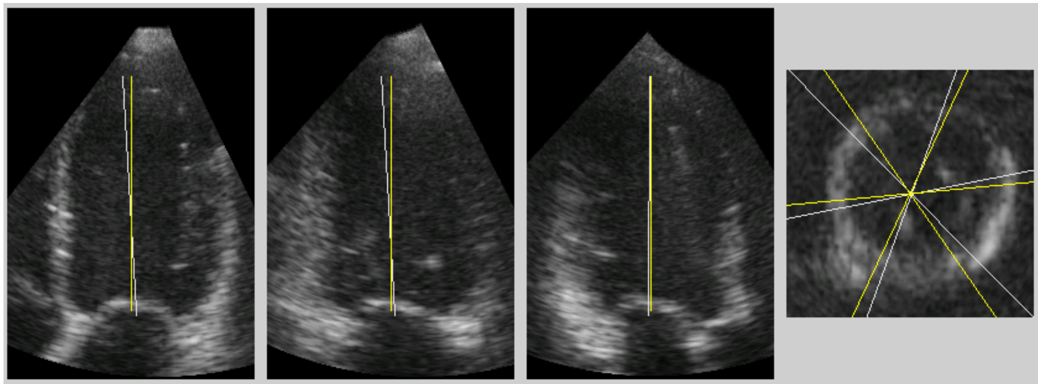

(a)

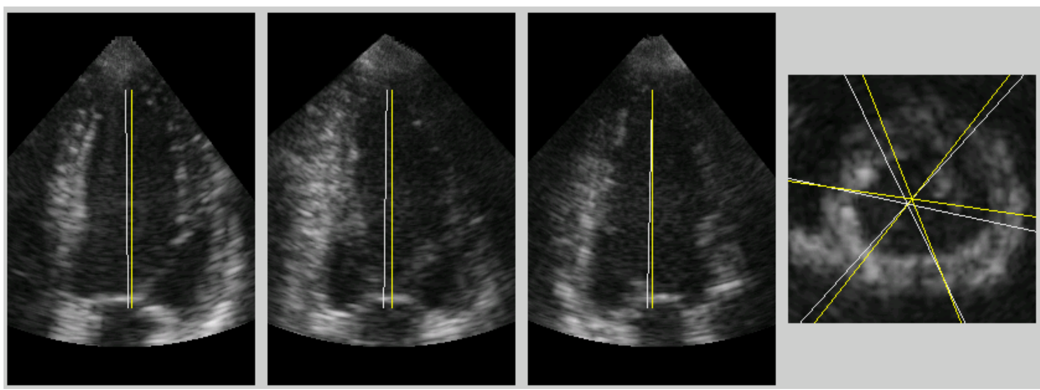

(b)

Figure 4: Two examples of extraction of standard 4CH, 2CH and LAX apical views, based on landmarks from the fitted model. Projected landmark lines from apex to base are superimposed on the apical views, and slice-direction lines are shown in the short-axis view. Yellow lines are from the proposed method, whereas reference lines are show in white.

of standard apical and short-axis slices, as well as reducing the problem of out-of-plane motion experienced in short-axis slices.

Results from a dataset of 35 recordings demonstrates the feasibility of this approach, both for aligning apical and short-axis slices. For short-axis alignment, slices from an example recording clearly shows the advantage of correcting the short-axis slices for out-of-plane motion in imaging the same myocardial tissue throughout the cycle. This effectively prevents basal short-axis slices from dropping down into the atria during systole, and papillary muscles appear more similar from frame to frame in corrected mid-wall slices. Example slices from two example recordings also shows how alignment of apical A4C, A2C and LAX can be performed based on an assumption of fixed angle between the slices, with comparison to manually annotated landmarks. Furthermore, a previous study[6] has shown that the Kalman tracking approach successfully tracked and segmented the left ventricle in 21 out of tested 21 3D echocardiograms. Hence, high robustness has previously been demonstrated.

Based on the results in table 1, one can see that basal/mitral valve detection is more accurate than apex detection. This corresponds well with the fact that manual apex identification is considered more difficult than manual mitral valve identification. As for rotations, table 2 shows that the assumption of 60 degree angle between the apical slices does not seem to hold for the LAX slice, which has much higher angle bias than the other apical slices. Adjusting the angle of the LAX slice relative to the other slices would reduce the alignment error, and should therefore be considered.

Compared to the results reported by Lu,[4] the rotation errors for the apical views in this paper are smaller. The error for the basal landmark is similar, while the error for the apical error is larger compared to.[4] It should

Alignment error	Apex	Mitral valve	A4C	A2C	LAX
Proposed	8.4 ± 3.5 mm	3.6 ± 1.8 mm	$8.4 \pm 7.4°$	$8.0 \pm 7.6°$	$11.8 \pm 8.5°$
Lu 2008[4]	4.5 ± 3.5 mm	3.6 ± 3.1 mm	$13.2 \pm 12.5°$	$15.2 \pm 13.0°$	$14.5 \pm 13.2°$
Leung 2008[5]	7.6 ± 4.8 mm	4.5 ± 2.9 mm	$6.3 \pm 4.6°$	N/A	N/A

Table 3: Comparison of results to known prior art on detection of standard views.

be noted that Lu used a much larger dataset (N=326) and undisclosed exclusion criteria, which makes a fair comparison difficult. Compared to the results reported by Leung[5] (N=20), the apex and base position errors are smaller, whereas Leung report better A4C angle agreement. It should be noted that the aim of Leung's paper was volume registration of stress 3d echocardiography, instead of detection of standard views, which might have influenced the results. Table 3 provides a comparison to the results to Lu and Leung.

REFERENCES

1. Sugeng, L., Weinert, L., and Lang, R. M., "Left ventricular assessment using real time three dimensional echocardiography," *Heart* **89**(90003), 29iii–36 (2003).
2. Veronesi, F., Corsi, C., Caiani, E., Sarti, A., and Lamberti, C., "Tracking of left ventricular long axis from real-time three-dimensional echocardiography using optical flow techniques," *Information Technology in Biomedicine, IEEE Transactions on* **10**, 174–181 (Jan. 2006).
3. van Stralen, M., Leung, K., Voormolen, M., de Jong, N., van der Steen, A., Reiber, J., and Bosch, J., "Time continuous detection of the left ventricular long axis and the mitral valve plane in 3-d echocardiography," *Ultrasound in Medicine & Biology* **34**, 196–207 (Feb. 2008).
4. Lu, X., Georgescu, B., Zheng, Y., Otsuki, J., and Comaniciu, D., "Autompr: Automatic detection of standard planes in 3D echocardiography," *Biomedical Imaging: From Nano to Macro, 2008. ISBI 2008. 5th IEEE International Symposium on* , 1279–1282 (May 2008).
5. Leung, K. Y. E., van Stralen, M., Nemes, A., Voormolen, M. M., van Burken, G., Geleijnse, M. L., ten Cate, F. J., Reiber, J. H. C., de Jong, N., van der Steen, A. F. W., and Bosch, J. G., "Sparse registration for three-dimensional stress echocardiography," *Medical Imaging, IEEE Transactions on* **27**, 1568–1579 (Nov. 2008).
6. Orderud, F. and Rabben, S. I., "Real-time 3D segmentation of the left ventricle using deformable subdivision surfaces," *Computer Vision and Pattern Recognition, CVPR. IEEE Conference on* (2008).
7. Orderud, F., Kiss, G., and Torp, H. G., "Automatic coupled segmentation of endo- and epicardial borders in 3D echocardiography," *to appear in Ultrasonics Symposium, 2008. IEEE* (2-5 Nov. 2008).
8. Bar-Shalom, Y., Li, X. R., and Kirubarajan, T., [*Estimation with Applications to Tracking and Navigation*], Wiley-Interscience (2001).
9. Doo, D. and Sabin, M., "Behaviour of recursive division surfaces near extraordinary points," *Computer-Aided Design* **10**, 356–360 (Nov. 1978).